NGL 50-002-044

THE SOFT X-RAY BACKGROUND AS A SUPERNOVA BLAST WAVE VIEWED FROM INSIDE: SOLAR ABUNDANCE MODELS

Richard J. Edgar

University of Wisconsin-Madison

Received: Accepted:

Running Title: SOFT X-RAY BACKGROUND: A MODEL

Subject Headings: interstellar: matter -- shock waves -- X-rays: general

ABSTRACT

A model of the soft X-ray background ($0.1 \lesssim h\nu < 0.284$ keV). is presented in which the Sun is assumed to be inside an active supernova blast wave. The blast wave, in turn, is evolving in a preexisting cavity. The broad-band surface brightnesses can be explained by such a blast wave with an explosion energy of $E_o \gtrsim 5 \times 10^{50}$ ergs and radius 80 to 100 pc, using solar abundances.

An approach to treating the problem of large anisotropies in the ambient medium is also explored, accommodating the observed anticorrelation between the soft X-ray surface brightness and the 21 cm column density. It is found that only for post shock temperatures below 10^6 K a shock propagating into a density enhancement will be dimmer than a similar shock in a lower density region.

I. Introduction

This work continues a project of modeling the soft X-ray background by the assumption that the Sun is inside an active blast wave. Cox and Anderson (1982; hereafter CA) produced such models in a uniform ambient medium, and found a set of dynamical parameters which gives a tolerable fit to the sky surveys of McCammon et al. (1983) and others. The present work makes an attempt to generalize the CA project, finding limits on the parameters in question. Using dynamical models of Cox and Edgar (1983; Paper I) and Edgar and Cox

(1984; Paper II), it is possible to examine the effects of a pre-existing cavity (say, from a previous supernova in the same vicinity) on a supernova blast wave.

The McCammon et. al. (1983) sky survey is presented in broad-band form. The two lowest energy bands, Boron (B-band; $0.1 \lesssim h\nu < 0.187$ keV) and Carbon (C-band; $0.1 \lesssim h\nu < 0.284$ keV), can be fit well by a model such as that discussed above. However, CA were unable to create a model which produces sufficient medium-energy (M-band; $0.4 \lesssim h\nu \lesssim 1.4$ keV) counts. While some substantial fraction of the observed M-band sky brightness may come from sources other than hot interstellar gas (for example dM stars or some extragalactic source; McCammon et. al. 1983), the M-band sky is remarkably isotropic outside of the Loop I/North Polar Spur complex, which suggests some local isotropic source such as a blast wave. Also, since the North Polar Spur is proposed (Borken and Iwan 1977, Iwan 1980) to be a re-heated supernova remnant (SNR), and it is clearly associated with an M-band enhancement, it is desirable to create a model which will produce more M-band flux than those of CA. Toward this end, and also with an eye toward examining reheated cavity models, the present work has focused mainly on blast waves propagating into pre-existing cavities. However, using the solar abundances of Ross and Aller (1976), our models are no more productive of M-band photons than those of CA.

Section II discusses the detailed numerical models and presents an analytical approximation to the predicted surface brightnesses in the B and C bands. Section III is an exposition of a scheme for examining a non-isotropic ambient medium in an attempt to model the observed anticorrelation between soft X-ray intensity and neutral hydogen column density. In section IV the results are summarized in a series of contour plots, and limits on the dynamical parameters are discussed.

II. Detailed Numerical Modeling

We have generated a modeling program which follows the dynamics of a blast wave using the dynamical model of Paper II, integrates the ionization balance equations using rates given by Raymond and Smith (1977, 1979), and then calculates the X-ray surface brightness. This is calculated in the form of binned spectra and integrated against band response functions, in particular those appropriate to the Wisconsin rocket detectors, as given by McCammon et al. (1983). We report here the band-integrated spectra, which facilitate comparison to existing sky survey data.

We have also included the preliminary response function for a Wisconsin rocket payload using beryllium filters to delimit the softest energy band ($0.07 \lesssim h\nu < 0.110$ keV). Preliminary results and a brief description of this payload are given by Sanders et al. (1984).

This model assumes that the post-shock ion and electron temperatures are equal (electrons being heated by non-Coulomb processes in the shock). Early in the life of the remnant, thermal conduction is important, and is accounted for as recommended by Cowie (1977), allowing for saturation effects. As the post-shock temperature drops with time, the thermal conductivity also drops, so the structure of the model remnant approaches that of an adiabatic blast wave (see, e.g. Sedov 1959, and Cox and Franco 1981).

The characteristic radius for the changeover from early conduction dominated behaviour (described by Paper I) to late adiabatic behaviour is called R_1. See Paper II for its prescription. It is frequently useful to parameterize the shock radius in units of R_1, introducing $z=R_s/R_1(E_{o,\omega},n_1)$. (The algebra is complicated in the case of a pre-existing cavity by the need to specify the density at some particular radius. It is most convenient to specify n_1, the ambient density at $R_s = R_1$, putting one in the odd position of calculating R_1 in terms of one of the parameters there.

The models assume a power-law ambient density, considering $n_o \propto R^{-\omega}$, with $\omega = 0$, -2, and -4 (uniform density and two steepnesses of pre-existing cavities). Solar abundances were used, and pre-shock ionization states were those of an equilibrium 1.0×10^4 K gas.

We find several interesting results, which tend to confirm those of CA. Perhaps most notable is that the various ions studied (all stages of the elements He, B, C, N, O, Ne, Mg, Si, S, Ca, Fe and Ni) are typically far from collisional equilibrium; time scales for ionization and recombination are comparable to the dynamical time scales. We also note that the ambient density is the most tightly constrained parameter, though the particular value one must assume to produce a desired surface brightness depends somewhat on the value assumed for ω.

Table 1 gives the dynamical properties of the runs that were done; the X-ray surface brightnesses (as viewed from the center) are given in Table 2. Nearly all the runs were for $\omega = -4$ since the

primary purpose of this effort was to examine the deviations from the CA calculations.

We have found an analytic approximation to both the C-band rates and the B/C ratio, which is useful for discussing the behavior of the results. The C-band approximation is a slight modification of the expressions given by Hamilton, Sarazin, and Chevalier (1983; HSC) and CA for the total luminosity of a blast wave (with $x_s = n_s/n_o$ as the density compression factor at the shock):

$$C \simeq 62 \frac{3}{3-\omega} \frac{x_s}{4} \left(\frac{n_o}{.004\ \mathrm{cm}^{-3}}\right)^2 \left(\frac{R_s}{100\ \mathrm{pc}}\right) L_{22} \qquad (2.1)$$

$$L_{22} = \max\left[1.3\left(\frac{T_s}{10^6 K}\right)^{-\frac{1}{2}},\right.$$

$$\left. 1.1\left(\frac{T_s}{10^6 K}\right)^{\frac{1}{4}} \left(\frac{1000\ \mathrm{cm}^{-3}\ \mathrm{yr}}{n_o t}\right)^{\frac{1}{2}} \exp\left(\frac{-8}{8-\omega} \frac{80\ \mathrm{cm}^{-3}\mathrm{yr}}{n_o t}\right)\right],$$

with a further factor of exp $(1-10^6 K/T_s)$ when $T_s < 10^6$ K. This last factor (the "cold correction") is an attempt to reproduce the fact that lower temperature plasmas tend to radiate in lower energy portions of the spectrum than the C-band. The various factors of this formula can be given physical interpretations as follows. The $T_6^{-1/2}$

(where $T_6 = T_s/10^6$ K) law is the equilibrium cooling coefficient of Raymond, Cox, and Smith (1976), appropriate when ionization stages are in approximate collisional equilibrium. The other alternative is the estimate by CA of a non-equilibrium cooling coefficient, modified by an exponential factor based on that of HSC which corrects for the finite time needed to reach ionization stages which will radiate soft X-rays. The ω-dependence was introduced to fit the $\omega = -4$ results of this paper, while preserving the $\omega = 0$ form of HSC. Further, an empirical fit to the B/C ratio produces

$$\frac{B}{C} = \min\left[0.58, \left(\frac{T_s}{8.55\times10^4 K}\right)^{-0.4386} \exp\left(\frac{80\ cm^{-3}\ yr}{n_o t}\right)\right]. \quad (2.2)$$

Since most of the runs in this work were done with $\omega = -4$, the ω-dependence of equation (2.2) should be taken as uncertain.

The results of these approximations as applied to the detailed runs are presented in Table 2. Also included are the percentage differences between the numerical models and the analytical approximations. While the agreement is only good to about 20%, the approximation preserves the general trends pointed to by the detailed models.

Figure 1 presents the results of the approximation for $\omega = -4$ and $E_o = 0.5 \times 10^{51}$ ergs in the form of a contour plot. The vertical axis is log T_s, the post-shock temperature. The horizontal axis is log n_1,

where n_1 is the normalizing density at $R_s = R_1$. It is a constant over the time development of a single blast wave, so a given blast wave will evolve straight down in this diagram. The contour lines are those of the C-band approximation of equation (2.1), and the plus signs are the various detailed runs, labeled with their run numbers. This entire diagram has E_o fixed at 0.5×10^{51} ergs. The kinks in the contour lines around $\log T_s = 6.0$ show the boundaries between the various approximation regimes (equilibrium or non-equilibrium cooling, and the cold correction $\exp(1-1/T_6)$ for $T_6 < 1$). In reality the transitions would be smoother, but it is useful to be able to see on the diagrams where the changes in the approximation occur.

Model 17 falls in a regime which is interesting for several reasons, so it will be described in detail here. The ionization state of the gas rises rapidly just behind the shock; oxygen ions will be given as an example. Moving inward from the edge, the fraction n(O VII)/n(O) rises to essentially unity by $R/R_s \approx 0.96$. O VII remains the dominant species to $R/R_s \approx 0.80$, including more than 99% of the mass. Nevertheless, there is enough O VI in the region $0.96 < R/R_s < 1.0$ to produce a column density of 3.6×10^{13} cm^{-2}. This O VI will have a temperature of approximately T_s (0.56×10^6 K in this case), a velocity of roughly 3/4 of the shock velocity, or about 150 km/s. Jenkins (1978a, b) used the Copernicus Satellite to observe O VI column densities toward 72 early-type stars at various distances from 85 pc to ~2 kpc. These measurements tend to show detections with column densities $N(O\ VI) \sim (1-2) \times 10^{13}$ cm^{-2}, with velocities near

zero (with a star-to-star dispersion of 26 km s^{-1}) and thermal widths indicative of temperatures around 3×10^5 K. Some of the stars show only upper limits of roughly this magnitude. There is some difficulty fitting stellar continua near these lines, so that very broad profiles might have been missed (Jenkins, 1984). The column density discrepancy will be discussed in a moment; the velocity problem remains unresolved.

Of the power radiated in the B and C bands, roughly 2/3 is emitted in a dozen lines of Si VII, Si VIII, Si IX, Mg VIII and Fe X. Hence the abundances assumed for these heavy elements are crucial to the calculations, as is the assumption that these elements are in the gas phase prior to being shocked. If these elements must be sputtered from silicate dust grains, they will probably not reach such high ionization stages as quickly, which might also make the emission less bright.

One problem that arises in the calculation of the numerical models is that they were assumed to be "non-radiative" (that is, radiation losses were neglected in the dynamical calculations). As the temperature becomes lower and lower, however, this assumption eventually fails (since gas with log T between 5 and 6 radiates with great efficiency [Raymond, Cox, and Smith, 1976]). In practice, the radiation rates for the various gas parcels were calculated only at the end of the remnant evolution (since we assumed for dynamical purposes that no radiation has taken place previously). Hence we are,

strictly speaking, unable to calculate the amount of energy previously radiated by a gas parcel. However, a reasonable approximation (and probably an overestimate) to this quantity can be obtained by multiplying the final radiation rate by the time since the parcel was shocked. This quantity can then be compared to kT, so that some idea can be formed concerning which parcels have cooled significantly. The resulting quantity typically rises quite sharply and then falls off steeply behind the shock, so that even though the calculation is very approximate, the actual result (namely the identification of cooled parcels) is not very sensitive to the details of the approximation.

Once the cooled parcels have been identified (and these are, where they exist at all, invariably near to the shock and few in number), they are excluded from the line integrals used in calculating the surface brightness. The runs marked in table 2 have been corrected in this manner.

This approximation probably yields excellent results for the C-band, and likely also the B-band, but not for softer X-rays which are emitted copiously by the cooler gas nearest the shock front (i.e. by gas with log T ~ 5.5), where the approximation is weakest.

This approach also provides an interesting insight into the O VI problem. CA found that the column densities of O VI predicted by their models were quite insensitive to all input parameters (other than the assumed pre-shock ionization state of the gas), and further that these were in excess of those reported by Jenkins (1978a, b). The present program suffers from the same effect. In the cooler

models, however, most of the O VI is in the outer shells which are identified by the above procedure as having cooled. It is expected that substantial recombination will have occurred in these regions beyond what our (non-radiative) models indicate. If one thus ignores the O VI which these models predict in gas parcels that in fact have cooled, the column densities of O VI are brought down to values of (1-2) x 10^{13} cm^{-2}, comparable to the limits of Jenkins (1978a, b).

III. Anisotropic Media and Isobarichrones

One obvious feature of the soft X-ray background is an anti-correlation between the B and C bands and neutral hydrogen column densities as measured at 21 cm. Sanders et. al. (1977) argue that this effect is not due to absorption of the X-rays by intervening neutral gas, since both the best-fit value and lack of energy dependence of the cross section fail to match those predicted by atomic physics. If the gas were clumped into optically thick clouds, an absorption picture can be made to work, but Jahoda et. al. (1985) find from their 21 cm observations that the gas is not sufficiently clumped to produce the observed anti-correlation with soft X-rays. An alternative model is proposed by Sanders et al. (1977) who point out that volume occupied by hot X-ray emitting gas is not occupied by neutral absorbing gas. Hence at a given galactic latitude, if in a given direction one observes a small 21 cm column density, more room is left for X-ray emitting gas, which increases the emission measure

and hence the surface brightness of soft X-rays. This model assumes a uniform emitting region.

The present work attempts to put more physical verisimilitude into this latter displacement picture. The cavity models suggested a scheme for examining in an approximate way, using paired spherically symmetric models, the effects of a non-isotropic ambient medium, such as one containing large clouds. While the blast wave interacts only with the front surface of the cloud, there is some reason to think (as in the displacement picture of Sanders et al.) that if the neutral material begins further from the Sun, there remains less room for it before the line of sight breaks out of the disk of the Galaxy, and hence the column density will be smaller. The models actually examine the effects on X-ray flux of the pre-shock density and the distance to the shock front.

Suppose the preexisting cavity has the same power-law density dependence in all directions, but with a larger constant of proportionality in some directions (toward "clouds") than others. Consider two directions A and B, with A being toward a denser region of the sky. Then let the ambient density laws be

$$n_{oA} = n_A R^{-\omega} \qquad (3.1)$$

$$n_{oB} = n_B R^{-\omega}$$

in the two directions, with $n_A > n_B$ and the same value of ω. A schematic diagram of this situation is presented in figure 2.

The interior temperatures (and hence the sound speed) are very high, so if two separate models are to be used to represent the same blast wave in these two directions, they share the same center and thus must have the same interior pressure. Further, they must have had the same interior pressure throughout their histories. The two models should thus be characterized by the same age. These two requirements suggest the name "Isobarichrones" for two such models: they have the same age and interior pressure history.

In Paper II it was shown that time and edge pressure develop approximately as power-laws with normalized radius z:

$$t \propto z^{(5-\omega)/2} \qquad (3.2)$$

$$p_s \propto z^{-3}.$$

Also, the central plateau pressure is always nearly one-third of the post-shock pressure, so that $p_c \propto z^{-3}$. Thus if two models are to have both the same age and pressure history, we are constrained to pairs with the same value of ω, as was assumed above.

As the two models evolve, there are two competing effects on their X-ray surface brightness. First, the higher density model A tends to be brighter for reasons discussed by CA, basically that more material enhances the emission measure. Second, since most of the X-ray power is in lines of highly ionized species, the degree of ionization is critical to the X-ray band surface brightnesses. Model A, since it has a higher ambient density, also has a lower shock velocity, and hence a lower post-shock temperature. The excitations then tend to favor lower energy transitions than model B, tending to make it less bright at higher energies.

To make this quantitative, let the ratio of the shock radii be given by the parameter λ (which is less than one in the present notation):

$$R_{sA} = \lambda R_{sB}. \qquad (3.3)$$

Since (Paper II) $E_o = 3V_s p_s \varepsilon(\omega)/2$ where V_s is the volume of the remnant, $\varepsilon(\omega)$ is a numerical factor that depends on ω (values are given in Paper II), and p_s and ω are the same for the two remnants,

$$E_{oA} = \lambda^3 E_{oB}. \qquad (3.4)$$

Thus the explosion energies will be different for isobarichrone model

pairs. Qualitatively this means that some of the energy originally directed toward the cloud (model A) has washed around the cloud (into the model B directions).

Using equations (27) and (28) of Paper II (with $\ell n\ \Lambda$ fixed) and eliminating R_1 and t_1 in favor of E_o and n_1 [where $n_o = n_1 z^{-\omega}$], a bit of algebra produces

$$n_{1A} = n_{1B}\ \lambda^{-\frac{14-\omega}{7-3\omega}},$$

$$z_A = z_B\ \lambda^{-\frac{5}{7-3\omega}}, \qquad (3.5)$$

$$n_{oA} = n_{oB}\lambda^{-2},$$

for the normalizing density n_1, the normalized shock radius z (which governs the maturity of the remnant with respect to thermal conduction), and the present-day ambient density n_o. The ideal gas law then produces the post-shock temperature law

$$x_{sA}\ T_{sA} = \lambda^2\ x_{sB}\ T_{sB}. \qquad (3.6)$$

(In these models, x_s approaches the familiar value of 4 at large z, in fact for z slightly greater than unity.)

Using the approximate C-band count rate function from section II above, it is possible to examine the behavior of the surface brightness by calculating the derivative $dC/d\lambda$. This can be done in each of the three regimes (non-equilibrium cooling, equilibrium cooling, and $T_s < 10^6$ K). This demonstrates that the first two cases produce brighter C-band rates in direction A (the "cloud"), i. e. that C correlates with n_o (and hence presumably with the column density N_H as viewed from inside the remnant). Only in the third case ($T_s < 10^6$ K) does one find the desired anti-correlation. In fact the "cold correction" factor $\exp(1-1/T_6)$ is responsible for this anti-correlation behavior. In other words, this approximation scheme predicts that when the post-shock temperature of remnant B is less than a million degrees, remnant A will be dimmer. This is borne out by several sets of detailed model calculations for isobarichrone sets.

Figure 3 is a contour plot which illustrates this situation for $E_{oB} = 5 \times 10^{50}$ ergs and $\omega = -4$. The axes are T_{SB}, the post-shock temperature of a remnant chosen here to have C = 200 counts per second (direction B), and R_{SA}, the minor shock radius (direction A). Applicable detailed model runs are plotted as plus signs and marked with their run numbers. Isobarichrone families of models fall along horizontal lines in this diagram, and runs 13 and 17 are "B" models corresponding to the "A" models 14 (for 13) and 18 and 19 (for 17).

The contour lines are the approximate C-band rates from equation (2.1). The 200 count s^{-1} contour which runs from upper left to lower right is the $\lambda = 1$ line, where the radii (and densities) in the two directions A and B are equal. To the left of this line, $\lambda < 1$, so $R_{SA} < R_{SB}$ and $n_{oA} > n_{oB}$. These contours show a ridge running from upper left to lower right, with a saddle at approximately the location of run 17. (The 200 count s^{-1} contours should cross at the saddle with $\lambda = 1$ following the more vertical one.) Thus below $T_{SB} = 10^6$ K, we have an anticorrelation between C and n_o (i. e. a smaller R_{SA} gives a smaller C-band rate), while the reverse is true above 10^6 K.

Clearly, since all this analysis was done with spherically symmetric models, this approximation is sufficiently crude that little if anything can be said about the edges of the clouds.

IV. A Summary: Contour Plots

As a summary of the behavior of the models we have calculated, and in an attempt to constrain the model parameters for the local bubble, we present several contour plots of parameter space. Equation (2.1) presents a manner of estimating the C-band intensity as a function of three parameters which (using the relations derived in Paper II) can be taken to be R_s, n_o, and E_o. Given these three parameters, all other dynamic quantities of interest can be calculated. In particular, we can calculate the postshock temperature T_s, the central pressure which the local interstellar medium might be expected to experience, and (using equation [2.2]) the B/C ratio.

The all-sky average value for the C-band intensity is approximately 200 counts s^{-1}. We have therefore set C = 200 for purposes of these plots, picked values for R_s and n_o, and iteratively solved for E_o. The other parameters then follow directly as above. The resulting contour plots are presented for several parameters as figure 4 (for $\omega = -4$).

Each plot has the post-shock temperature contours plotted for reference (labeled with the temperature in units of 10^6 K) in dashed lines. Figure 4a also has contours of $E_{51} = E_o/10^{51}$ ergs. The upper right part of these diagrams is the "cool" portion, where the cold correction $\exp(1-1/T_6)$ is used. In the lower left, the non-equilibrium cooling approximation was used. The shaded portion of these figures represents a fold in the surface: all of the approximation regimes coexist in this area. In other words, for some choices of R_s and n_o, there are three choices of E_o (and hence T_s and the other parameters) which will produce C = 200, depending on which approximate cooling function one chooses. The $T_6 = 1$ contour is in the shaded fold zone.

In the extreme upper right part of these diagrams ($T_6 \leq 0.4$), the edge of the blast wave will have cooled, so both the analytical approximation (equation 2.1) and the models on which it is based will fail.

Several authors (see Paresce 1984 and references therein) have observed that the Sun seems to be in a cavity of extent ~100 pc in most directions. These results come from UV absorption line studies

and extinction measurements. We thus expect that the radius of the present blast wave will be of this order. Figure 4a demonstrates that an explosion energy of 5×10^{50} ergs or more is needed for such a radius.

In order for the isobarichrone scheme of section III to produce an anticorrelation of C-band intensity with the neutral hydorgen column density N_H, we need $T_6 < 1$, which is the upper right part of these diagrams.

Figure 4b shows contours of the central pressure, expressed for convenience as p/1000k, where k is the Boltzmann constant. It then has units of cm^{-3} K. This plot tends to force our attention toward the upper right, in order to reduce the overpressure needed within the local bubble. Various estimates of the mean interstellar pressure produce p/k values of order 2000 cm^{-3} K (e. g. Spitzer 1978), and while we expect a large overpressure within an active blast wave, the value of p/k = 30,000 cm^{-3} K required by this plot for a post shock temperature of 10^6 K seems uncomfortably high. However, such high pressures have been proposed before (e.g. Williamson et al. 1974, Shapiro and Field 1976). Jenkins (1984) points out that while the Sun seems to be embedded in a very local partially ionized medium with $T \simeq 1\text{-}2 \times 10^4$ K and $n \simeq 0.1$ cm^{-3}, so that $p/k \simeq 2000$ cm^{-3} K, the extent of this region (3-4 pc in some directions [Bruhweiler and Kondo 1982]) plus its sound speed make the shock crossing time of order 10^5 yr, which is comparable to the dynamical timescales of the present

bubble models. Thus the discrepancy in the pressures may be an effect no more transient than the blast wave itself.

Figure 4c presents a contour plot of the B/C ratio, and it is apparent that this ratio is an excellent temperature diagnostic. The local component of the soft X-ray background seems to have a B/C ratio of between 0.35 and 0.45 (Nousek et al. 1982), which constrains T_s to the range 0.6 to 1.0 x 10^6 K.

We thus find ourselves constrained to a rather narrow stripe of parameter space. If one wishes to fit the B/C band without overly stressing the pressure constraints, and one wishes to use the isobarichrone anticorrelation scheme of section II, one is forced to the conclusion that T_s is (.8 ±.2) x 10^6 K. We consider it an important success of this model that the anticorrelation scheme works in a temperature regime which is allowed by the observed B/C ratio. Note also that the acceptable values of n_o represented are in a narrow range; we find that for C = 200 counts s^{-1} (with $\omega = -4$, 80 pc $\lesssim R_s \lesssim$ 120 pc, and $0.6 < T_6 < 1.0$), we require ambient densities of (1.2 ± .2) × 10^{-2} cm^{-3}.

For other values of ω the approximation formula (2.1) has not been checked as rigorously against detailed models. The diagrams in figure 5 are similar to those in figure 4, only for the $\omega = 0$ or uniform ambient density case, again with C fixed at 200 cps. These plots, and similar diagrams for $\omega = -2$, suggest ambient density ranges of (0.7 ± .2) × 10^{-2} cm^{-3} for $\omega = 0$ and (0.9 ± .2) × 10^{-2} cm^{-3} for $\omega = -2$. The temperature constraints are independent of ω, producing

$T_s = (0.8 \pm .2) \times 10^6$ K, though the isobarichrone scheme of section III will not work as envisioned in the uniform medium ($\omega = 0$) case.

Several questions were suggested by the investigation of CA, some of which are addressed by the present project. Among these quesions are the following:

(1) CA produced a set of SNR parameters (n_o, R_s, and t) that fit the B and C band data for $E_o = 5 \times 10^{50}$ ergs. What ranges can these parameters take on without substantially impacting on the quality of the fit? How would these ranges change if E_o were allowed to vary? The range of parameters has been addressed above.

(2) Is it possible (for example, by setting off the explosion in a pre-existing cavity) to make models that will produce a more significant fraction of the observed M-band flux? The present work suggests that explosions in cavities are no more productive of M-band X-rays than those in uniform ambient media. This still presents no serious difficulty to the local bubble models, but will be more serious in attempting to model the North Polar Spur region, which is potentially such a large bubble viewed from the outside.

(3) Are there parameter choices for which the X-rays could be produced without at the same time generating a large local O VI component? It is still true that the active blast wave models inherently generate N(O VI) ~ 2 to 5×10^{13} cm^{-2}. This component is hot, has large radial velocity, and is found only along a thin zone

close to the shock. If, however, the edge of the blast wave has cooled, it seems likely that it will have also recombined to stages below O VI. This appears promising, though more detailed models which incorporate radiation effects in a more natural and satisfactory manner would shed more light on the question.

This work was supported in part by NASA grant number NGL 50-002-044 at the University of Wisconsin-Madison. I would like to thank Don Cox for much helpful advice, and Wilt Sanders for numerous useful discussions and criticisms, as well as Steve Snowden, Keith Jahoda, John Mathis, Dan McCammon and Bill Kraushaar for refusing to understand what was poorly explained.

References

Borken, R. J. and Iwan, D. C. 1977, Ap.J., 218, 511.

Bruhweiler, F. C., and Kondo, Y. 1981, Ap.J., 259, 232.

Cowie, L. L. 1977, Ap.J., 215, 226.

Cox, D. P., and Anderson, P. R. 1982, Ap.J., 211, 268 (CA).

Cox, D. P., and Edgar, R. J. 1983, Ap.J., 265, 443 (Paper I).

Cox, D. P., and Franco, J. 1981, Ap.J., 251, 687 (CF).

Edgar, R. J., and Cox, D. P. 1984, Ap.J., 283, 833 (Paper II).

Hamilton, A. J. S., Sarazin, C. L., and Chevalier, R. A. 1983, Ap.J.Supp., 51, 115 (HSC).

Iwan, D. C. 1980, Ap.J., 239, 316.

Jahoda, K., McCammon, D., Dickey, J. M., and Lockman, F. J. 1985, Ap.J., 290, 229.

Jenkins, E. B. 1978a, Ap.J., 219, 845.

Jenkins, E. B. 1978b, Ap.J., 220, 107.

Jenkins, E. B. 1984, in I.A.U. Colloquium No. 81: The Local Interstellar Medium, ed. Y. Kondo, F. C. Bruhweiler, and B. D. Savage, (Washington: NASA), p. 155.

McCammon, D., Burrows, D. N., Sanders, W. T., and Kraushaar, W. L. 1983, Ap.J., 269, 107.

Nousek, J. A., Fried, P. M., Sanders, W. T. , and Kraushaar, W. L. 1982, Ap.J., 258, 83.

Raymond, J., Cox, D. P., and Smith, B. W. 1976, Ap.J., 204, 290.

Raymond, J., and Smith, B. W. 1977, Ap.J.Supp., 35, 419.

Raymond, J., and Smith, B. W. 1979, private communication (update of Raymond and Smith 1977).

Ross, J. E. and Aller, L. H. 1976, Science, 191, 1223.

Sanders, W. T., Kraushaar, W. L., Nousek, J. A., and Fried, P. M. 1977, Ap.J. (Letters), 217, L87.

Sanders, W. T., Snowden, S. L., Bloch, J. J., Juda, M., Jahoda, K. M. and McCammon, D. 1984, in I.A.U. Colloquium No. 81: The Local Interstellar Medium, ed. Y. Kondo, F. C. Bruhweiler, and B. D. Savage, (Washington: NASA), p. 222.

Sedov L. I. 1959, Similarity and Dimensional Methods in Mechanics (New York: Academic).

Shapiro, P. R., and Field, G. B., 1976 Ap.J., 205, 762.

Spitzer, L. 1978, Physical Processes in the Interstellar Medium (New York:Wiley).

Williamson, F. O., Sanders, W. T., Kraushaar, W. L., McCammon, D., Borken, R. and Bunner, A. N. 1974, Ap.J. (Letters), 193, L133.

Figure Captions

Fig. 1. The analytical approximation of equation (2.1) as a contour plot of C-band surface brightness in counts s^{-1}. The vertical axis is log T_s, the post-shock temperature. The horizontal axis is log n_1, the normalizing density of Paper II, which is a constant over the life of a given remnant. $E_o = 0.5 \times 10^{51}$ ergs, and $\omega = -4$ (i.e. $n_o \propto R^4$). Also plotted are the positions of applicable model runs, with their run numbers. A remnant evolves straight down on this diagram.

Fig. 2. A schematic representation of the cavity discussed in section III. Direction A represents a pre-existing cloud.

Fig. 3. A contour plot of the C-band intensity in direction A (see Fig. 2). Axes are log T_{sB}, the post-shock temperature in direction B (which is taken to have C = 200 counts s^{-1}), and R_{sA}, the shock radius in direction A. Applicable runs are plotted. Isobarichrone models fall on horizontal lines in this diagram. $E_o = 0.5 \times 10^{51}$ ergs, and $\omega = -4$.

Fig. 4. For C = 200 counts s^{-1}, contours of the post-shock temperature T_6 (dashed lines, all plots) in units of 10^6K are presented. The shaded region represents a fold in the surface. Axes are shock radius and current ambient density. $\omega = -4$.

a) Explosion energy $E_{51} = E_o/10^{51}$ ergs in solid lines. b) Pressure p/1000k in solid lines. c) Boron to Carbon band ratio B/C in solid lines.

Fig. 5. Same as Fig. 4, only for $\omega = 0$. $C = 200$ counts s^{-1} as before.

Table 1
DYNAMICAL PROPERTIES AND N(O VI)

Run	R_s	n_o	T_s	t	z	x_s	E_o	N(O VI)
	pc 10^{-3}	cm^{-3}	10^6 K	10^5 yr			10^{51} erg	10^{13} cm^{-2}
			Time Sequence A ($\omega = -4$)					
5	83.9	2.48	4.33	0.36	0.800	2.782	0.500	...
10	94.0	3.90	1.91	0.60	0.896	2.858	0.500	3.1
1	104.6	6.00	0.77	0.98	0.998	3.353	0.500	...
11	110.0	7.32	0.48	1.24	1.049	3.769	0.500	4.9
9	120.0	10.37	0.25	1.87	1.145	3.966	0.500	6.7
6	136.0	17.10	0.10	3.35	1.298	3.997	0.500	...
			Time Sequence B ($\omega = -4$)					
8	58.0	5.86	5.56	0.22	0.800	2.782	0.500	...
12	62.1	7.70	3.41	0.30	0.859	2.809	0.500	2.8
7	96.1	44.30	0.11	2.27	1.327	4.000	0.500	...
			An Isobarichrone Pair ($\omega = -4$)					
13	75.0	11.9	1.08	0.602	0.984	3.238	0.500	2.1
14	56.3	21.2	0.51	0.613	1.052	3.831	0.211	4.2
			An Isobarichrone Triplet ($\omega = -4$)					
17	83.7	14.1	0.56	0.874	1.053	3.789	0.500	3.6
18	62.8	25.1	0.30	0.888	1.135	3.960	0.211	2.8[a]
19	54.4	33.4	0.23	0.894	1.179	3.981	0.137	1.0[a]
			Miscellaneous Runs ($\omega = -4$)					
15	64.5	6.13	1.56	0.450	0.918	2.906	0.211	3.2
16	90.0	15.96	3.86	1.125	1.102	3.927	0.500	6.7
			A Uniform Ambient Density Case ($\omega = 0$)					
20	55.7	5.00	5.11	0.382	0.519	3.255	0.500	0.26

[a] These figures exclude cooled gas near the shock.

Table 2
BAND RATES

Run	Detailed Models Be	B	C	M	Analytical Approximation B	C	% B	% C
			Time Sequence A					
5	1.1	5.5	14.0	0.90	7.2	17.1	30.3	22.4
10	1.8	11.4	31.7	1.12	12.1	34.3	6.1	8.1
1	9.7	31.8	57.2	1.15	23.1	54.7	-27.3	-4.4
11	6.4	25.7	50.1	0.54	29.0	58.8	12.7	17.4
9	8.4	19.4	32.1	0.36	15.9	26.3	-18.1	-18.1
6	3.4	6.9	12.1	0.17				
			Time Sequence B					
8	12.5	17.5	55.2	7.10	20.1	69.6	15.1	26.1
12	4.3	33.0	113.6	11.80	28.0	101.7	-15.0	-10.5
7	17.4	32.2	56.5	1.38				
			An Isobarichrone Pair					
13	7.8	66.3	196.9	5.60	56.4	158.9	-14.9	-19.3
14	30.0	124.1	254.2	3.95	130.1	277.4	4.8	9.1
			An Isobarichrone Triplet					
17	18.8	87.7	189.2	3.15	91.9	204.2	4.8	7.9
18	29.2[a]	77.3[a]	137.7[a]	2.11[a]	88.2	149.2	14.1	8.4
19	13.9[a]	51.0[a]	102.4[a]	1.67[a]	50.9	85.4	-0.2	-16.6
			Miscellaneous Runs					
15	4.1	23.6	59.3	1.40	19.4	53.0	-18.0	-10.7
16	25.9	76.1	138.2	2.13	83.5	157.1	9.8	13.7
			A Uniform Ambient Density Case					
20	2.4	34.8	136.1	35.70	27.0	108.7	-22.3	-20.2

[a] These figures exclude cooled gas parcels near the shock.

Richard J. Edgar: Department of Astronomy, University of Virginia,
Charlottesville, VA 22903.

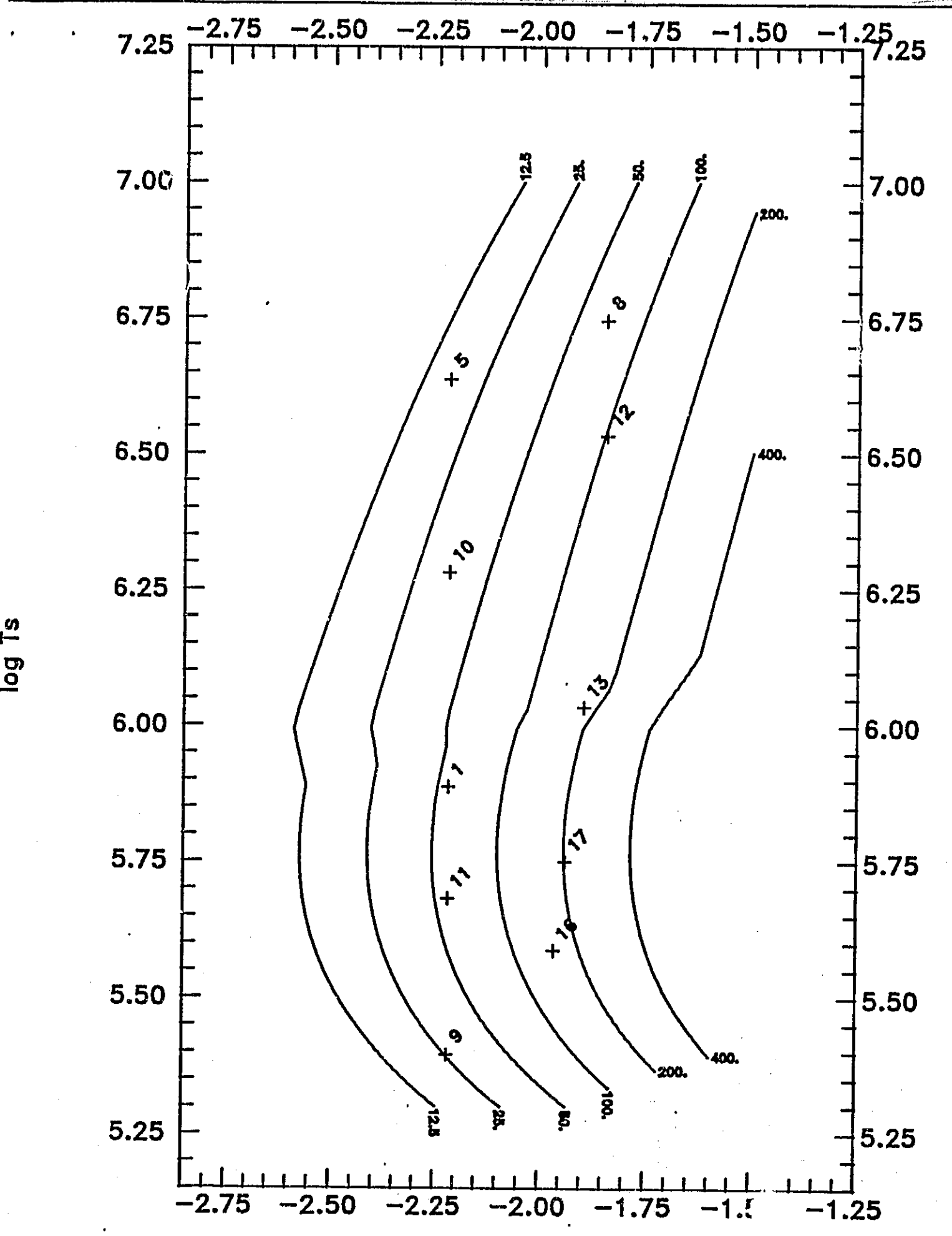
−2.75 −2.50 −2.25 −2.00 −1.75 −1.50 −1.25
7.25
7.00
6.75
6.50
6.25
6.00
5.75
5.50
5.25
log Ts
log n1
12.5
25.
50.
100.
200.
400.
+5
+8
+10
+12
+1
+13
+11
+17
+16
+9

Figure 1

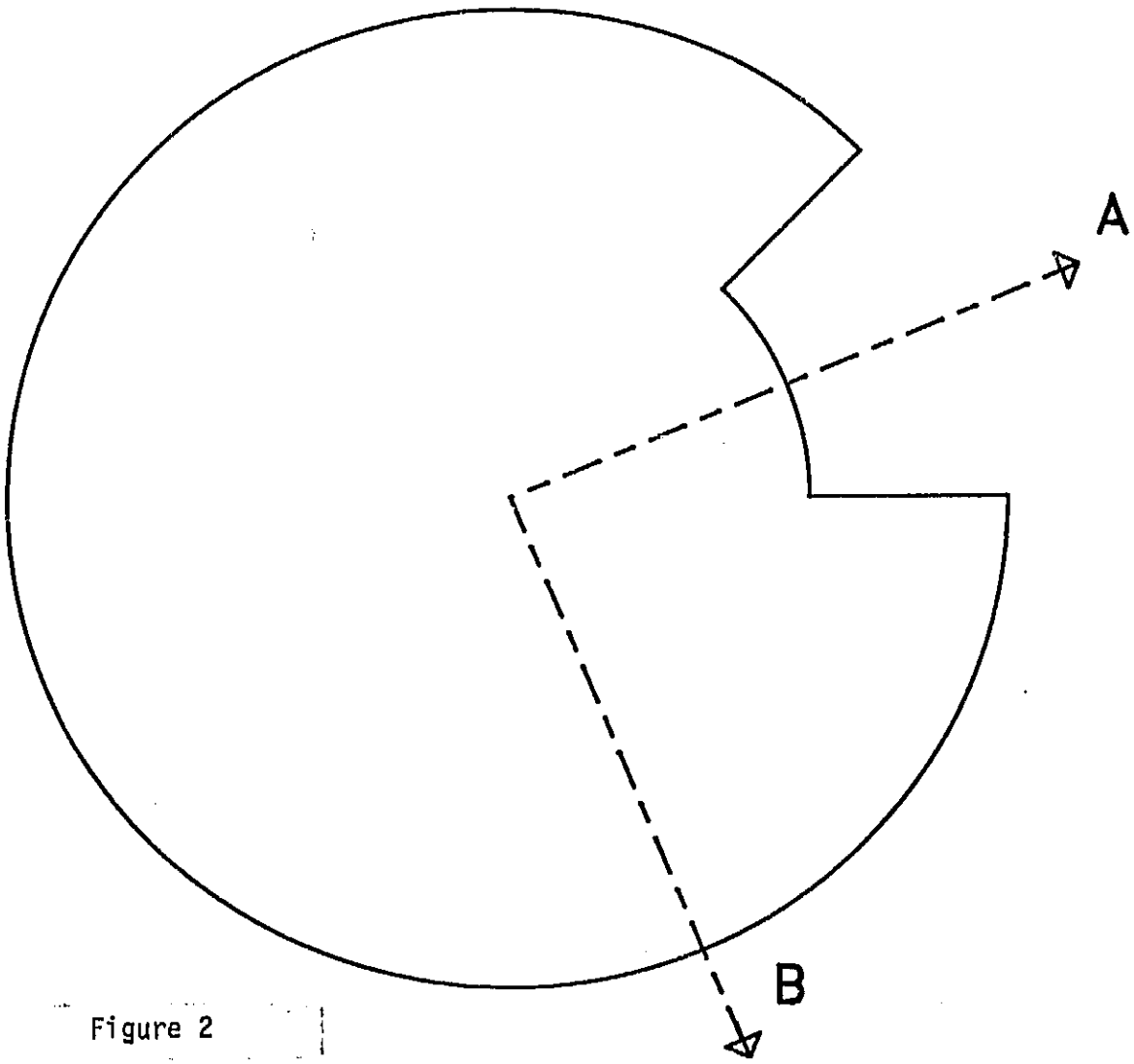

Figure 2

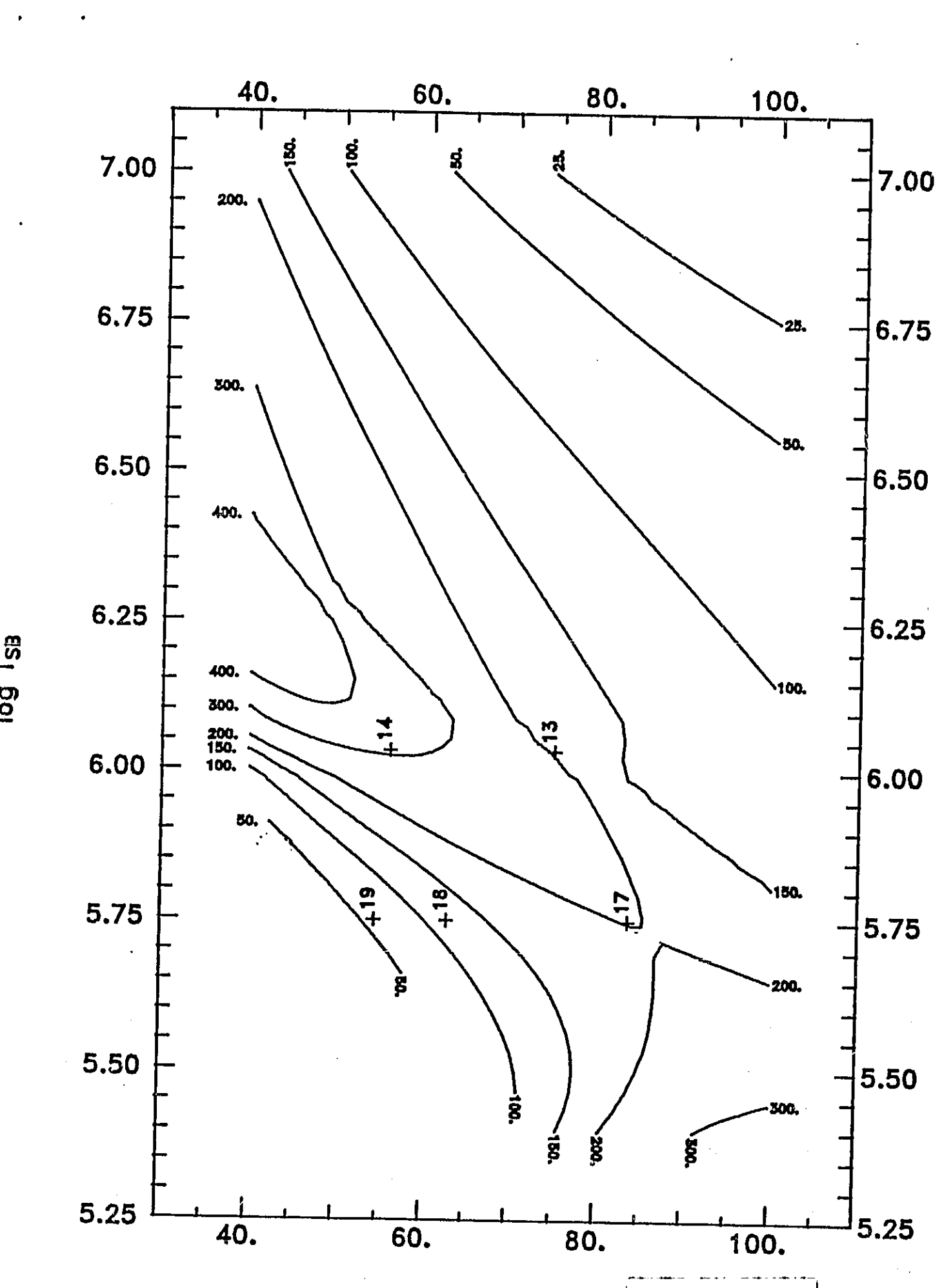
40.
60.
80.
100.
7.00
6.75
6.50
6.25
6.00
5.75
5.50
5.25
log I_{SB}
R_{SA} (pc)
150.
100.
50.
25.
200.
300.
400.
+14
+13
+17
+19
+18

Figure 3

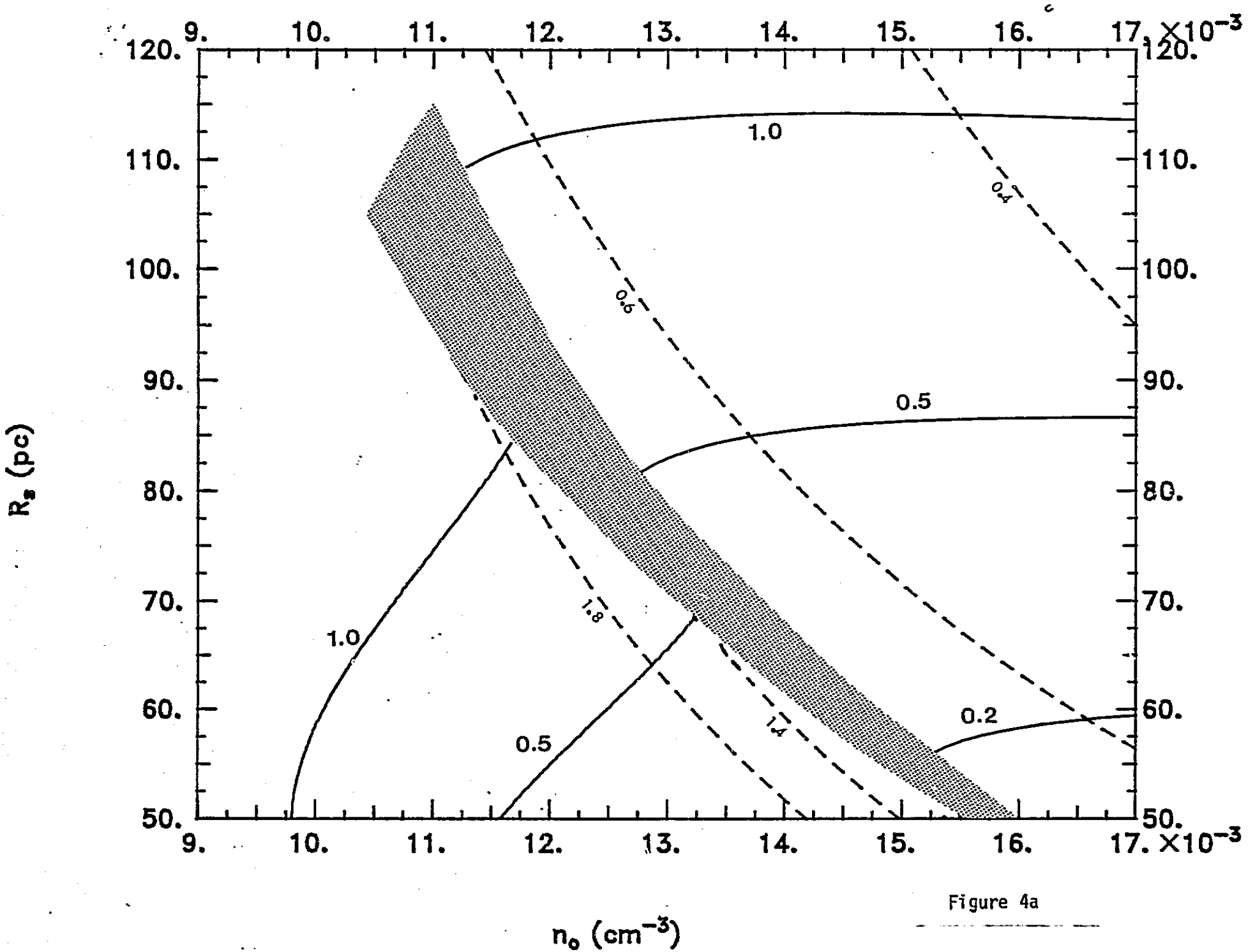
9.
10.
11.
12.
13.
14.
15.
16.
17. X10⁻³
120.
110.
100.
90.
80.
70.
60.
50.
1.0
0.5
0.2
0.4
0.6
1.8
1.4
R_s (pc)
n_o (cm⁻³)

Figure 4a

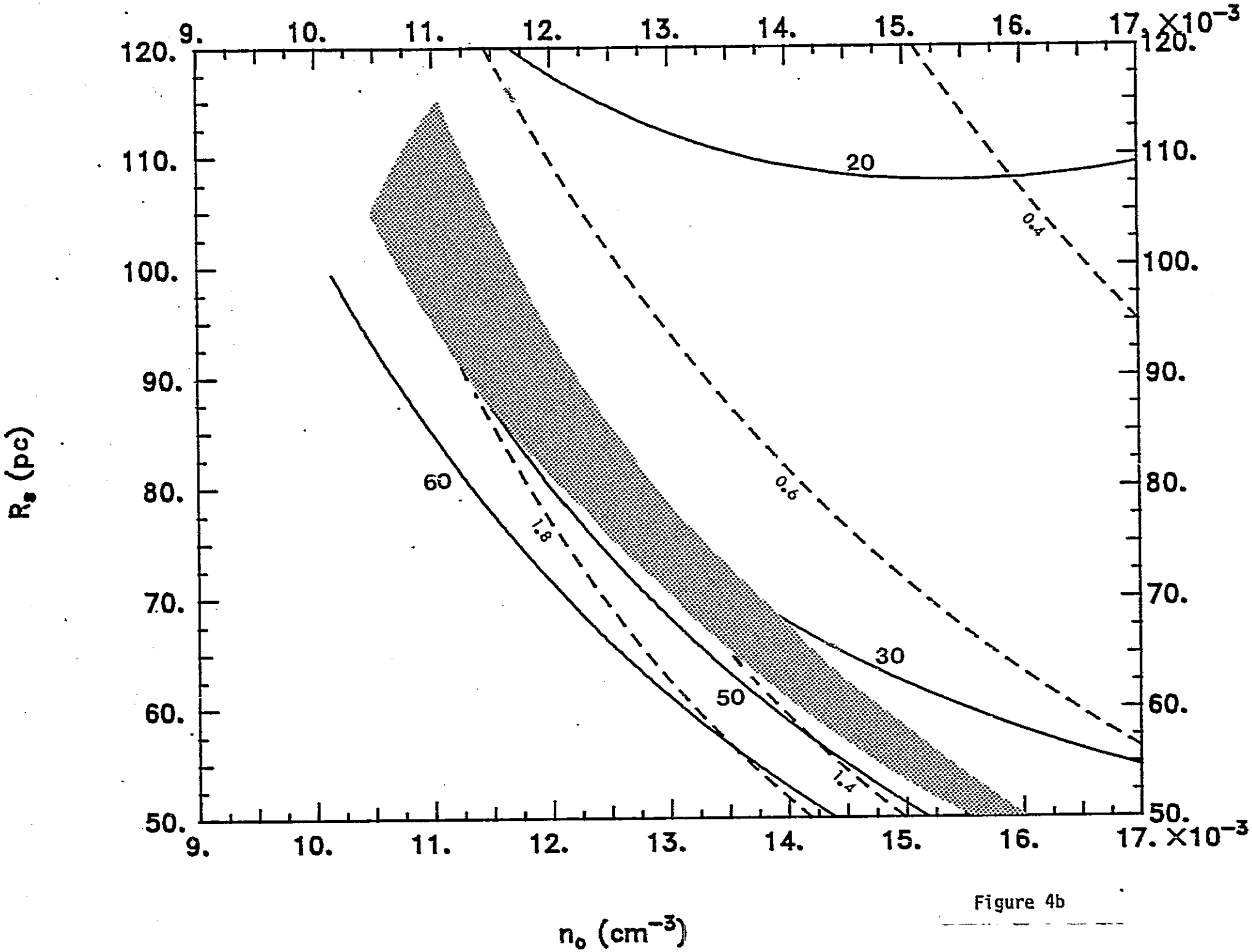
9.
10.
11.
12.
13.
14.
15.
16.
17. X10⁻³
120.
110.
100.
90.
80.
70.
60.
50.
20
0.4
0.6
60
1.8
30
50
1.4
Rs (pc)
no (cm⁻³)

Figure 4b

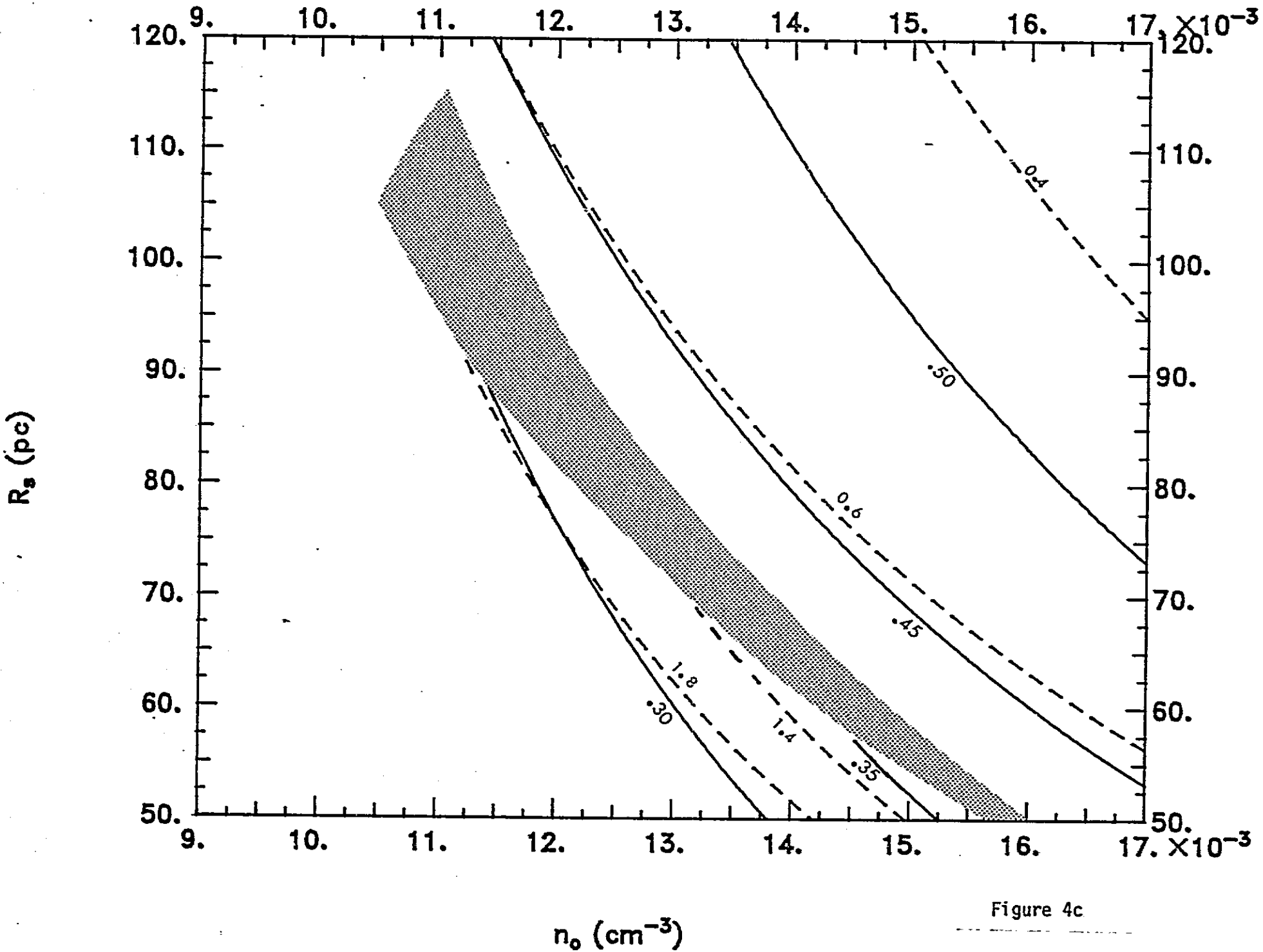
9.
10.
11.
12.
13.
14.
15.
16.
17. X10^-3
120.
110.
100.
90.
80.
70.
60.
50.
R_s (pc)
n_o (cm^-3)
.50
0.6
0.4
.45
1.8
1.4
.30
.35

Figure 4c

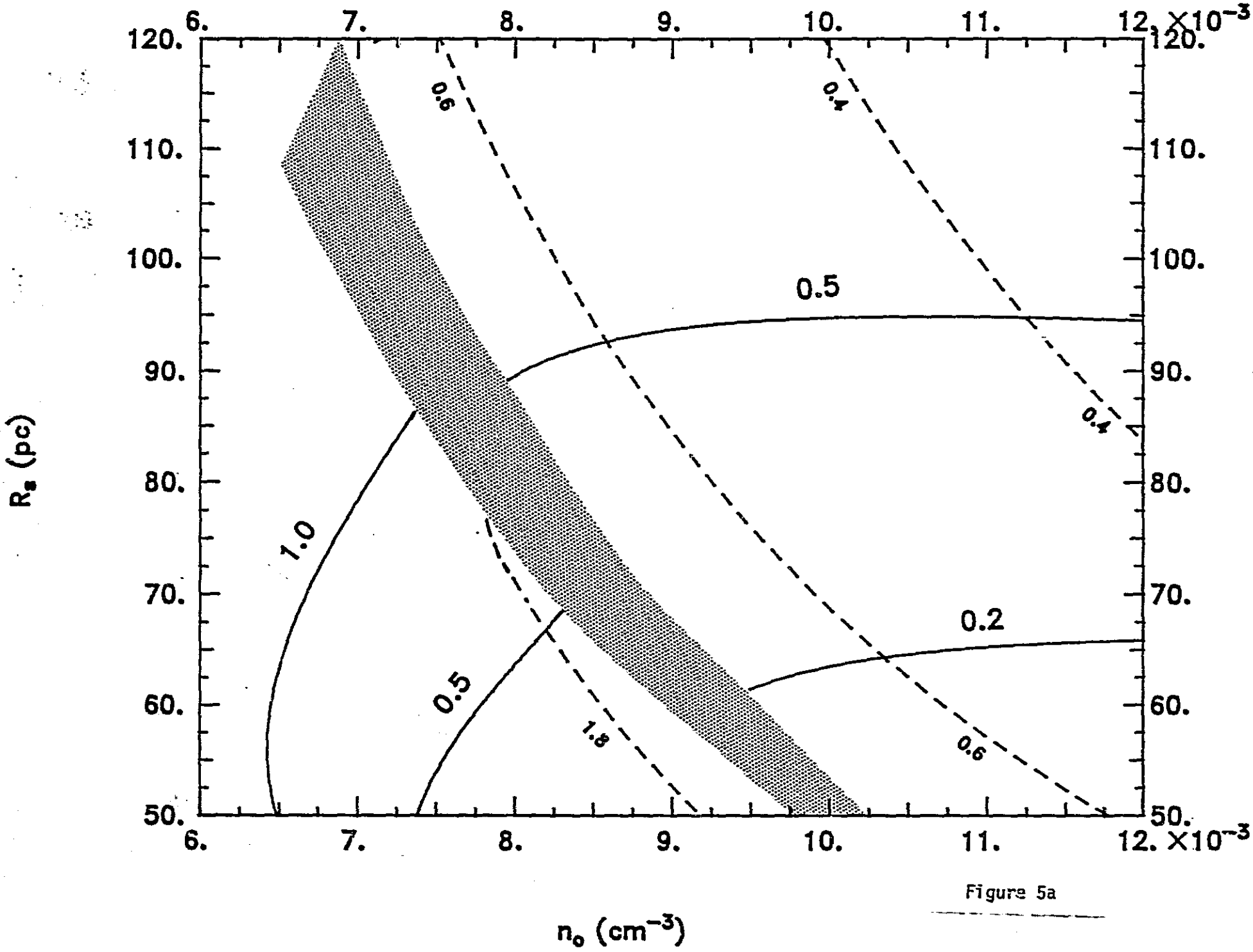
6.
7.
8.
9.
10.
11.
12. X10^-3
120.
110.
100.
90.
80.
70.
60.
50.
R_s (pc)
n_o (cm^-3)
0.6
0.4
0.5
0.4
1.0
0.2
0.5
1.8
0.6

Figure 5a

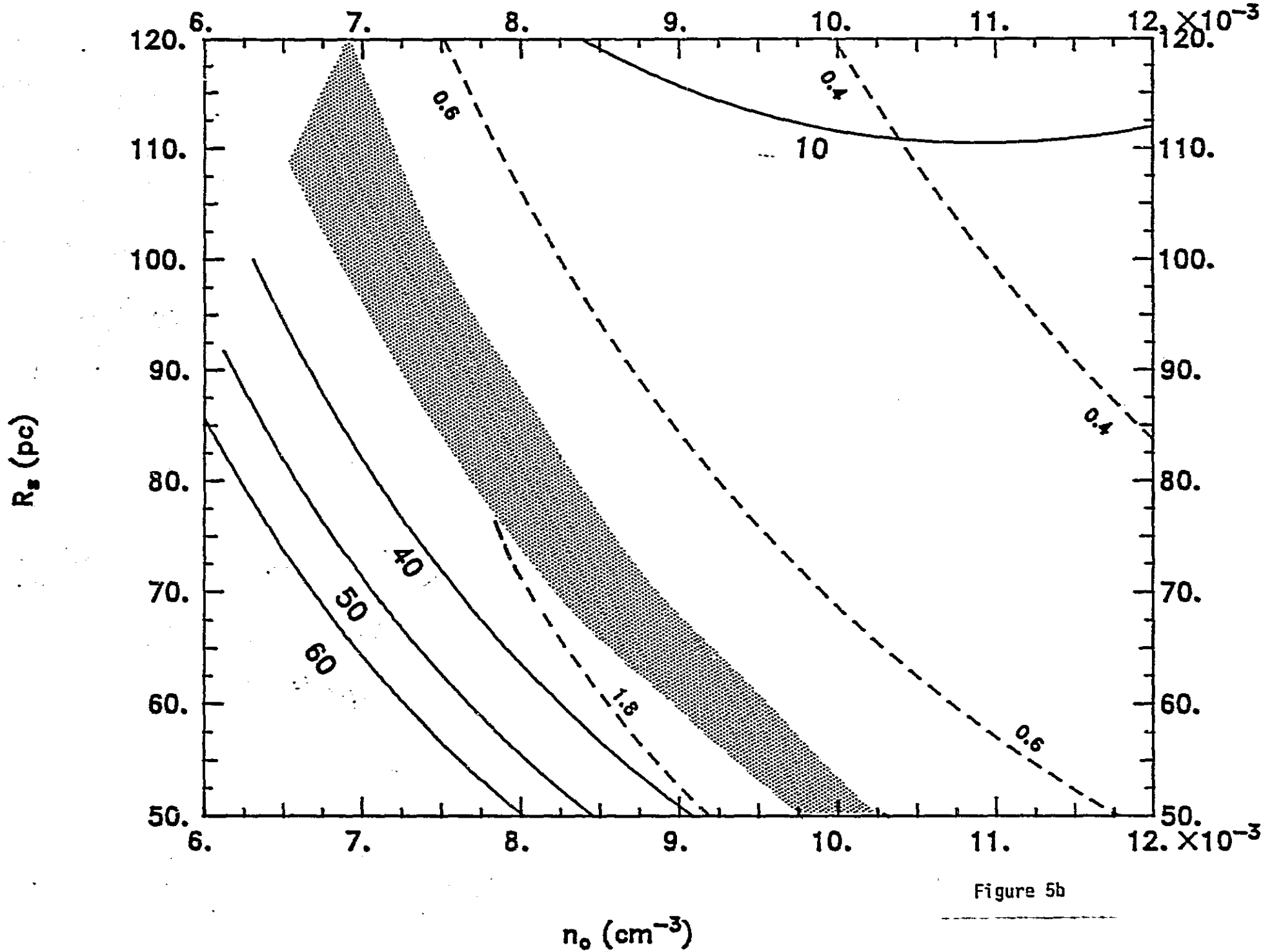
6.
7.
8.
9.
10.
11.
12. X10^-3
120.
110.
100.
90.
80.
70.
60.
50.
R_s (pc)
n_o (cm^-3)
0.6
0.4
10
40
50
60
1.8
0.4
0.6

Figure 5b

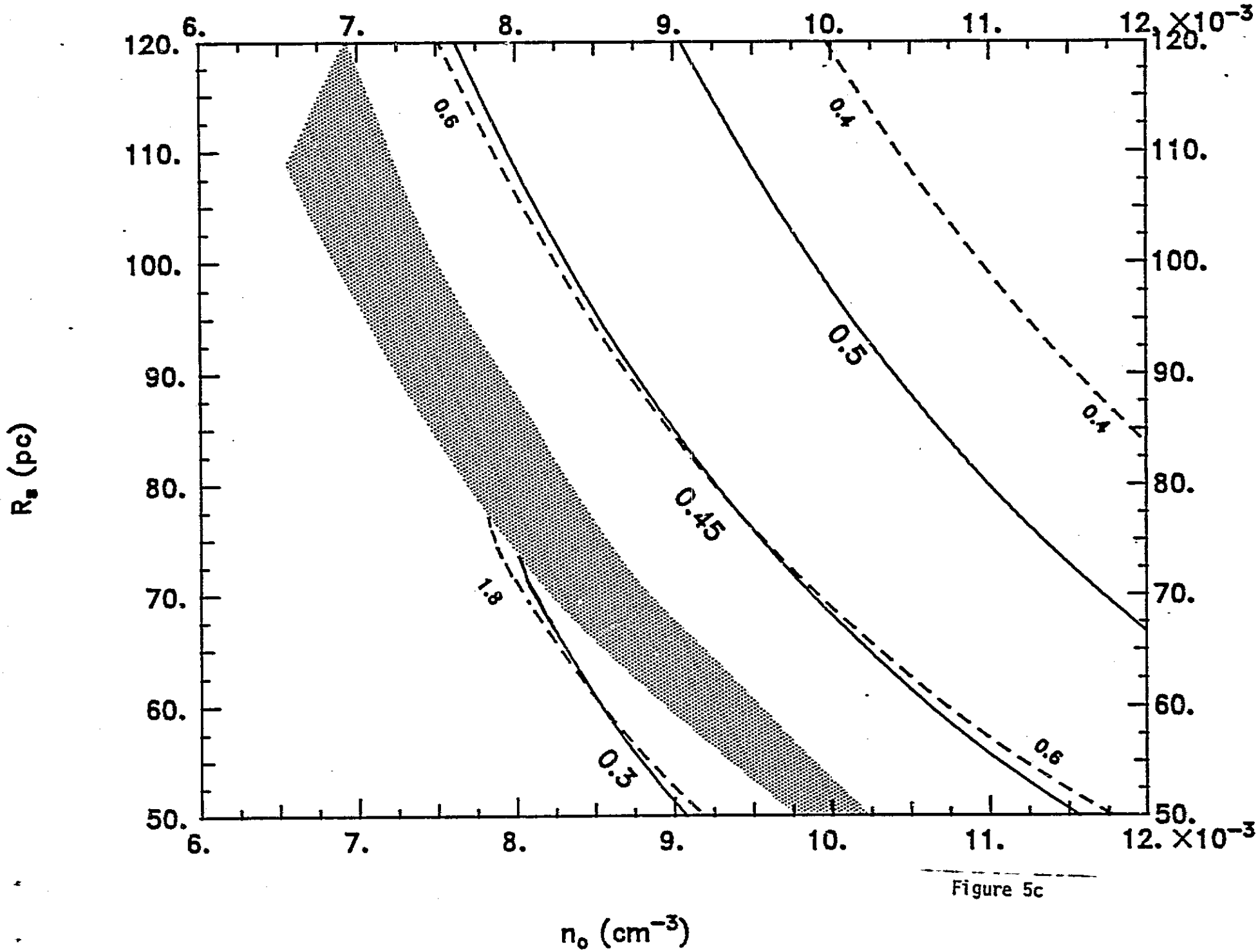
6.
7.
8.
9.
10.
11.
12. ×10⁻³
120.
110.
100.
90.
80.
70.
60.
50.
0.6
0.4
0.5
0.4
0.45
1.8
0.6
0.3
R_s (pc)
n_o (cm⁻³)

Figure 5c